Brain Abnormalities in a Neuroligin3 R451C Knockin Mouse Model Associated With Autism

Jacob Ellegood, Jason P. Lerch, and R. Mark Henkelman

Magnetic resonance imaging (MRI) has been used quite extensively for examining morphological changes in human and animal brains. One of the many advantages to examining mouse models of human autism is that we are able to examine single gene targets, like that of Neuroligin3 R451C knockin (NL3 KI), which has been directly implicated in human autism. The NL3 KI mouse model has marked volume differences in many different structures in the brain: gray matter structures, such as the hippocampus, the striatum, and the thalamus, were all found to be smaller in the NL3 KI. Further, many white matter structures were found to be significantly smaller, such as the cerebral peduncle, corpus callosum, fornix/fimbria, and internal capsule. Fractional anisotropy measurements in these structures were also measured, and no differences were found. The volume changes in the white matter regions, therefore, are not due to a general breakdown in the microstructure of the tissue and seem to be caused by fewer axons or less mature axons. A larger radial diffusivity was also found in localized regions of the corpus callosum and cerebellum. The corpus callosal changes are particularly interesting as the thinning (or reduced volume) of the corpus callosum is a consistent finding in autism. This suggests that the NL3 KI model may be useful for examining white matter changes associated with autism. ***Autism Res*** *2011,4:xxx–xxx*. © 2011 International Society for Autism Research, Wiley Periodicals, Inc.

Keywords: animal models; magnetic resonance imaging; diffusion tensor imaging; neuroligin3; volume assessment

Introduction

Autism is a highly heterogeneous disorder both in its clinical presentation and in the genetic background of autistic individuals. Marked by its heterogeneity, autism is characterized by three core behavioral symptoms: impaired social interaction, communication deficits, and repetitive, restrictive behaviors [Reiss, 2009]. In 2005, it was reported that approximately 6 in 1,000 people have an autism spectrum disorder or ASD [Fombonne, 2005], which includes classic autism, Asperger's syndrome, pervasive developmental disorder not otherwise specified, Rett syndrome, and childhood disintegrative disorder. Further, ASDs are increasingly being diagnosed [Baird et al., 2006]. Within autism, there is a known genetic linkage. It has been shown in twin studies that there is a 90% concordance rate with identical twins and a $>10\%$ rate with fraternal twins or siblings [Bailey et al., 1995; Steffenburg et al., 1989]. More than 35 genes have been identified as linked to autism in a recent publication [Abrahams & Geschwind, 2010a,b]. One of those 35 genes is Neuroligin3 (NL3).

The Neuroligin and Neurexin genes are synaptic cell adhesion genes; these genes and the corresponding scaffold proteins (SHANK genes) have been associated with Autism [Jamain et al., 2003; Laumonnier et al., 2004], schizophrenia [Kirov et al., 2008], Tourette's syndrome [Lawson-Yuen, Saldivar, Sommer, & Picker, 2008], and mental retardation [Zahir et al., 2008]. Specific disruptions in these genes have been recognized in autism association studies [Jamain et al., 2003; Laumonnier et al., 2004]. One of these studies found an inherited mutation in NL3 in a family with two brothers, one with typical autism and the other with Asperger's syndrome. This mutation replaced a highly conserved arginine residue with cysteine at amino acid position 451 (R451C) [Jamain et al., 2003], which caused a decrease in NL3. To investigate the possible mechanism of this mutation, Tabuchi et al. [2007] introduced the R451C substitution into a mouse model, thus creating the NL3 R451C knockin (NL3 KI) mouse model associated with autism. Behavioral studies on this mouse model have been performed [Chadman et al., 2008; Tabuchi et al., 2007], with conflicting results. Tabuchi et al. [2007] found that the NL3 KI mice had impaired social behaviors, but enhanced spatial learning abilities, whereas Chadman et al. [2008] found no such changes. Despite these conflicting results, the NL3 KI model allows both the examination of a specific model of human autism in the mouse, and the ability to examine neuroanatomical changes in this model.

From the Mouse Imaging Centre (MICe), Hospital for Sick Children, Toronto, Ontario, Canada (J.E., J.P.L., R.M.H.)

Address for correspondence and reprints: Jacob Ellegood, Mouse Imaging Centre (MICe), Hospital for Sick Children, Toronto Centre for Phenogenomics, 25 Orde Street, Toronto, Ontario, Canada M5T 3H7. E-mail: jacob@phenogenomics.ca

Grant sponsor: Canadian Institute for Health Research (CIHR); Grant number: MOP-106418; Grant sponsor: Ontario Mental Health Foundation (OMHF).

Published online in Wiley Online Library (wileyonlinelibrary.com)

DOI: 10.1002/aur.215

Magnetic resonance imaging (MRI) has been used quite extensively for examining volume changes in human and animal brains. A recent meta-analysis summarized the current volume changes in human autism [Stanfield et al., 2008]. That review found that the total brain size, cerebral hemispheres, cerebellum, caudate nucleus, and corpus callosum are all affected in autism, and the effects were often age and IQ dependent [Stanfield et al., 2008]. Measuring volume changes with MRI in mouse models of autism have only been examined in a few studies [Nag et al., 2009; Radyushkin et al., 2009]. One of those studies looked at volume changes in the NL3 knockout mouse model [Radyushkin et al., 2009]. However, MRI volume measurements were not the primary focus of that article, and therefore, only gross anatomical structures were measured. Recently, using MRI volume changes in the mouse, investigators have shown left/right asymmetries [Spring et al., 2010], male/female neuroanatomy differences [Spring, Lerch, & Henkelman, 2007], as well as learning and memory changes [Lerch et al., 2011]. These same MRI techniques have been applied to disease models such as Alzheimer's [Lau et al., 2008] and Huntington's disease [Lerch et al., 2008]. Volume measurements with MRI have also been shown to be consistent with stereological measures [Lerch et al., 2008; Spring et al., 2010]. Further assessment of neuroanatomical change can be measured using an MRI technique called Diffusion Tensor Imaging (DTI). DTI enables the measurement of the diffusion properties of water, which allows one to look at the underlying cellular microstructure and orientation in the brain quantitatively. DTI studies in human autism have shown promise in detecting abnormalities in white matter structure, most notably in the corpus callosum [Alexander et al., 2007b]. While DTI has been used to examine differences in a mouse model of Fragile X Syndrome [Ellegood et al., 2010], currently no DTI studies have been performed on a mouse model specifically related to human autism.

One of the many advantages to examining mouse models of human autism is that we are able to determine the effects of a single gene, like NL3. This provides less confounding information, as the mice are genetically identical aside from the targeted gene. Further, the environment of all mice can be rigorously controlled, such that environmental influences are minimized. MRI studies in human autism are plagued by the genetic heterogeneity of the human population and environmental factors. Compounding the issue, human studies often use high functioning individuals (for the ease of the MRI examination), which may not be consistent with severe autistic individuals. Certainly, there are disadvantages to using mouse models. For one, changes found in a mouse model of autism do not necessarily mean those changes will be found in the human autism. Second, we will never find a specific mouse model that will encompass all the symptoms of human autism; there may never be a truly ''autistic mouse.'' Finally, single gene disorders and rare mutations, which are suitable for examination in mice, only account for a small fraction of human autistic cases [Abrahams & Geschwind, 2010a].

The NL3 KI mouse, does however, provide an ideal model for investigating a specific example of human autism, and the corresponding changes caused by the genetic manipulation. It can also provide insight into autism as a whole. The purpose of this study is to examine volumetric and white matter structural changes in the brain of the NL3 KI mouse model of autism, using high-resolution MRI and detailed quantitative and statistical analyses.

Methods

Specimen Preparation

Sixteen male mice were purchased from Jackson Labs (Bar Harbor, Maine), 8 NL3 KI mice (JAX ♯008475), and 8 WT mice (JAX ♯101045); all mice were on a mixed C57BL/6 and 129 background. The NL3 KI mutation was backcrossed for three to nine generations, as reported by Jackson Labs. These mice were sacrificed at postnatal day 108. Initially, the mice were anesthetized with ketamine/xylazine and intracardially perfused with 30 mL of 0.1 M PBS containing 10 U/mL heparin (Phamaceutical Partners of Canada (PPC), Richmond Hill, Ontario, Canada) and 2 mM ProHance (a Gadolinium contrast agent) followed by 30 mL of 4% paraformaldehyde (PFA) containing 2 mM ProHance [Spring et al., 2007]. Perfusions were performed with a Pharmacia minipump at a rate of approximately 100 mL/hr. After perfusion, mice were decapitated and the skin, lower jaw, ears, and the cartilaginous nose tip were removed. The brain within the skull was incubated in 4% PFA+2 mM ProHance overnight at 4°C then transferred to 0.1 M PBS containing 2 mM ProHance and 0.02% sodium azide for at least 7 days but not more than 2 months before MRI scanning.

Magnetic Resonance Imaging

A 7.0-T MRI scanner (Varian Inc., Palo Alto, CA) with a 6-cm inner bore diameter insert gradient (max gradient 100 G/cm, rise time = 150 μsec) was used for all MRI scans. Three custom built solenoid coils were used to image three brains in parallel [Bock, Nieman, Bishop, & Mark Henkelman, 2005]. Parameters used for anatomical MRI scans were optimized for high efficiency and gray/white matter contrast: T2-weighted, 3D fast spin echo, with a TR of 325 msec, and TEs of 10 msec per echo for six echoes, with the centre of k-space being acquired on the fourth echo, four averages, field-of-view of $14 \times 14 \times 25\,mm^3$ and matrix size of $432 \times 432 \times 780$

giving an image with 0.032-mm isotropic voxels. Total imaging time for this MRI sequence was ~12 hr [Henkelman, Baghdadi, & Sled, 2006].

DTI scanning was performed with a 3D diffusion-weighted fast spin echo sequence. DTI parameters: echo train length of 6, TR of 325 msec, first TE 30 msec, and a TE of 6 msec for the remaining five echoes, with the centre of k-space being acquired on the second echo, ten averages, field-of-view of $14 \times 14 \times 25\ mm^3$ and a matrix size of $120 \times 120 \times 214$ yielding an image with 0.117-mm isotropic voxels. One $b = 0\ s/mm^2$ image (with minimal diffusion weighting) and six high *b*-value images ($b = 1{,}956\ s/mm^2$) were acquired in six different directions [(1,1,0),(1,0,1),(0,1,1),(−1,1,0),(−1,0,1),(0,1,−1)] of (G_x, G_y, G_z). Total imaging time for this sequence was ~16 hr. DTI parameters were then calculated in every voxel to create maps of the mean diffusivity (MD), axial diffusivity (AD), radial diffusivity (RD), and fractional anisotropy (FA) [Alexander et al., 2007a; Le Bihan et al., 2001].

FA is a measure of the order of water diffusion in the given environment, and is a number ranging from 0 to 1. An FA of 0 indicates that the diffusion is isotropic, meaning that the diffusion of water molecules is equal in all directions; this is seen in solution, where the FA ~0, and in the gray matter where the barriers that restrict diffusion are spherically symmetric or lack order, FA ~0.2 to 0.5. An FA close to 1 indicates that the diffusion is anisotropic, meaning that the water molecules will primarily travel along a single preferred direction; this is seen in the white matter, where the water molecules would rather travel parallel to the axons than across. MD, AD, and RD are all related. MD is a measure of the average diffusion of the water molecules over all directions, AD measures the diffusion along the preferred direction of travel, and RD measures the average diffusion orthogonal to that preferred direction.

Registration and Analysis

To visualize and compare any changes in the NL3 KI mouse, the brains (from the anatomical scan as well as a separate registration for the $b = 0\ s/mm^2$ images from the DTI scans) are linearly (6 parameter followed by a 12 parameter) and then nonlinearly registered such that a transform is created for each mouse. All scans are then resampled with the appropriate transform and averaged to create a population atlas representing the average anatomy of the study sample. All registrations are performed using the mni_autoreg tools [Collins, Neelin, Peters, & Evans, 1994]. The result of the registration is to have all scans deformed into exact alignment with each other in an unbiased fashion. This allows for the analysis of the deformations needed to take each individual mouse's anatomy into the final atlas space, the goal being to model how the deformation fields relate to genotype [Lerch et al., 2008; Nieman, Flenniken, Adamson, Henkelman, & Sled, 2006]. The determinants of the deformation fields were then calculated as measures of volume at each voxel. Significant volume changes can then be calculated by warping a pre-existing classified MRI atlas onto the population atlas [Dorr et al., 2008], which allows the volume of 62 segmented structures encompassing cortical lobes, large white matter structures (i.e. corpus callosum), ventricles, cerebellum, brain stem, and olfactory bulbs [Dorr et al., 2008] to be assessed in all 16 brains. The volumes were calculated both as an absolute volume (mm^3) and a relative volume (percentage of total brain volume). For the DTI data set, the transformations applied to the $b = 0\ s/mm^2$ images during the registration process were applied to the FA, MD, AD, and RD maps for each brain, from which average maps were calculated for both the NL3 KI and the WT mouse. These values were then compared, and differences were assessed by measuring the mean values within the same 62 regions assessed in the anatomical MRI measurements and on a voxel-by-voxel basis. Multiple comparisons were controlled for using a False Discovery Rate (FDR) [Genovese, Lazar, & Nichols, 2002].

Results

Volume Measurements

The total brain volume for NL3 KI mouse brains, which included all 62 segmented structures [Dorr et al., 2008], was found to be smaller (−8%, FDR = 0.12). Further, the white matter volume (18 of 62 regions) and the gray matter volume (41 of 62 regions) were also found to be smaller by 10% (FDR = 0.06) and 8% (FDR = 0.13), respectively. The ventricles (3 of 62 regions) did not change significantly (FDR = 0.86). Of the 62 segmented structures, 20 were found to be significantly different at an FDR of $< 10\%$ when absolute volumes were compared, and 21% when relative volumes were evaluated. Eleven regions had both absolute and relative volume changes that were significant. Table I provides a representative sampling of the volume changes in specific structures. Several gray matter structures were found to be smaller in the NL3 KI mouse compared with the wild type. Examples would include the hippocampus (−12%, FDR = 0.06), the striatum (−12%, FDR = 0.06), and the thalamus (−15%, FDR = 0.04). Also, large white matter structures were found to be markedly smaller, such as the cerebral peduncle (−13%, FDR = 0.05), corpus callosum (−14%, FDR = 0.03), fornix (−14%, FDR = 0.02), fimbria (−12%, FDR = 0.06), and internal capsule (−15%, FDR = 0.04), contributing substantially to the overall white matter deficit.

Table I. Representative Volume Differences in the NL3 KI Mouse Model of Autism

	Volume (mean ± SD) Absolute (mm^3)			
Region	WT	NL3 KI	% Change	FDR
Amygdala	13.5 ± 1.2	12.6 ± 1.2	−6.7	0.27
Cerebral cortex—frontal lobe	43.0 ± 3.1	38.7 ± 3.5	−10.0	0.08
Cerebral cortex—occipital lobe	5.77 ± 0.64	5.26 ± 0.52	−8.8	0.20
Cerebral cortex—parieto-temporal lobe	73.3 ± 6.5	65.3 ± 6.5	−11.0	0.09
Cerebral peduncle	2.41 ± 0.19	2.10 ± 0.19	−12.9	0.05
Corpus callosum	20.8 ± 1.4	17.8 ± 1.6	−14.3	0.03
Fimbria	3.38 ± 0.33	2.98 ± 0.21	−11.9	0.06
Fornix	0.80 ± 0.05	0.69 ± 0.06	−14.3	0.02
Globus pallidus	3.19 ± 0.25	2.92 ± 0.26	−8.6	0.14
Hippocampus	21.3 ± 2.0	18.7 ± 1.5	−12.3	0.06
Internal capsule	3.45 ± 0.26	2.93 ± 0.32	−15.0	0.04
Striatum	21.6 ± 1.5	19.1 ± 1.7	−11.6	0.06
Thalamus	17.6 ± 1.4	15.1 ± 1.6	−14.6	0.04
White matter (18 regions)	58.6 ± 4.0	52.7 ± 4.4	−10.0	0.06
Gray matter (41 regions)	414 ± 31	380 ± 32	−8.3	0.13
Ventricles (three regions)	5.02 ± 0.66	5.07 ± 0.46	1.2	0.86
Total brain volume (62 regions)	478 ± 35	438 ± 36	−8.4	0.12

NL3 KI, neuroligin3 R451C knockin; FDR, false discovery rate.

Figure 1A shows three axial images of the consensus average of the 16 brains. Overlaid on these images are the significant differences on a voxel-by-voxel basis of the NL3 KI mouse compared with the wild type, any voxel highlighted was determined to be significantly smaller in the NL3 KI compared to the wild type at an FDR of <0.10. Several areas in the hippocampus were found to be significantly smaller, as seen in all three axial slices in Figure 1A. Similarly, specific areas in the striatum and cortex were also noted to be smaller in the NL3 KI (Fig. 1A, middle).

Diffusion Tensor Imaging

FA, MD, AD, and RD values were calculated in each of the same 62 regions used in the volume measurements. No significant differences were found in the mean FA of the regions examined in the NL3 KI compared with the wild type. However, Figure 1B shows the same three axial slices in Figure 1A as FA maps. Highlighted in Figure 1B are the FA differences on a voxel-by-voxel basis. Significantly smaller FA values were found at FDR values <0.10 in one spot in the right hemisphere of the globus pallidus. In fact, when the FDR threshold was lowered to an FDR of <0.20, the globus pallidus was found to have a smaller FA bilaterally, seen in Figure 1B (left).

There were no significant differences in MD or AD when either the mean values in the 62 regions or voxel-wise differences were examined. However, the RD was larger in 25 of the 62 regions at an FDR threshold of <0.15. Significantly larger RD values are highlighted in Figure 2 on the registered average of the RD maps (FDR of <0.10). In the posterior section of the corpus callosum (right) and also in the cerebellum in all three slices, significantly larger RD values can clearly be seen. The corpus callosum had a 10% larger RD (FDR = 0.12) in the NL3 KI compared with the WT and the cerebellar cortex and arbor-vita of the cerebellum (the white matter) has 11% (FDR = 0.11) and 12% (FDR = 0.11) larger RD values, respectively. Larger RD values were found in multiple other regions, such as the frontal (+7%, FDR = 0.12), parieto-temporal (+7%, FDR = 0.12), and occipital lobe (+8%, FDR = 0.11), as well as the hippocampus (+8%, FDR = 0.11) and thalamus (+8%, FDR = 0.12).

Discussion

As mentioned briefly in the introduction, previous volumetric measurements using MRI have been attempted on the NL3 KO mouse model. However, with low resolution and poor SNR Radyushkin et al. were only able to manually delineate large structures such as the total brain (excluding the olfactory bulbs, cerebellum, and brain stem), lateral and third ventricles, the cerebellum, olfactory bulbs, and brain stem [Radyushkin et al., 2009]. The total brain volume in that study was found to be 5% smaller. This is consistent with what has been found in this study, where the total brain volume for NL3 KI mouse brains, which included all 62 segmented structures, was also found to be smaller (−8%, FDR = 0.12).

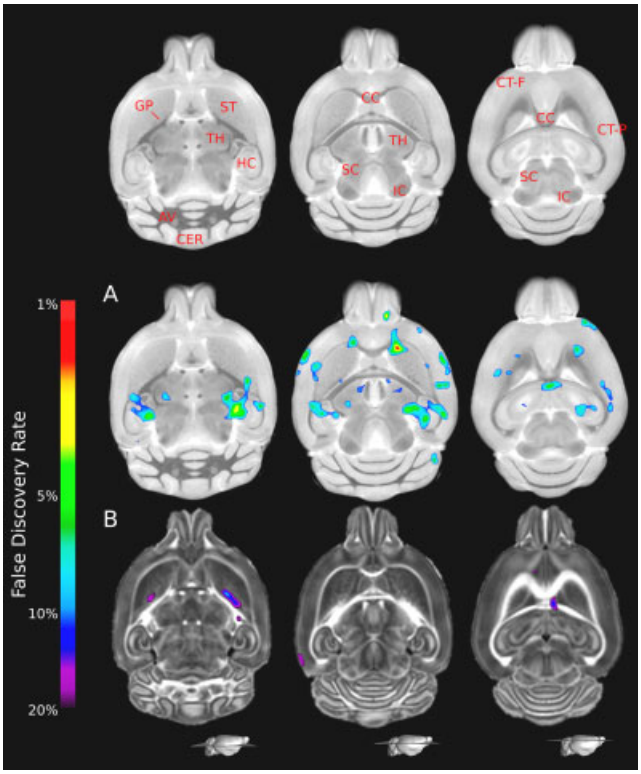

Figure 1. (**A**) Three axial slices from the consensus average of the 16 brains used in this study. Highlighted in A are the significantly different voxels indicating that the volume in the colored region is smaller in the NL3 KI compared to the wild type mouse. These differences are thresholded at a 10% false discovery rate. (**B**) The same three axial slices from the consensus average of the FA maps for all the 16 brains used in the study. Highlighted in B are significantly smaller FA values on a voxel-by-voxel basis; these changes are thresholded at a false discovery rate of 20%. Arbor-Vita of the cerebellum (AV), cerebellar cortex (CER), colliculus: inferior (IC), colliculus: superior (SC), cerebral cortex – frontal lobe (CT-F), cerebral cortex – parieto-temporal lobe (CT-P), globus pallidus (GP), hippocampus (HC), striatum (ST), and thalamus (TH). FA, fractional anisotropy; NL3 KI, neuroligin3 R451C knockin.

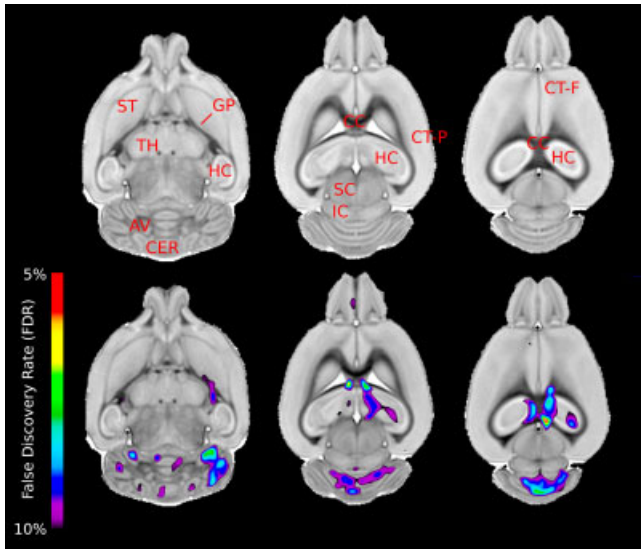

Figure 2. Three axial slices from the consensus average of the RD maps for the 16 brains used in this study. Highlighted are the significantly different voxels indicating a larger RD in the NL3 KI mouse in that region. These changes are thresholded at 10% false discovery rate. Arbor-Vita of the cerebellum (AV), cerebellar cortex (CER), colliculus: inferior (IC), colliculus: superior (SC), cerebral cortex—frontal lobe (CT-F), cerebral cortex—parieto-temporal lobe (CT-P), globus pallidus (GP), hippocampus (HC), striatum (ST), and thalamus (TH). RD, radial diffusivity; NL3 KI, neuroligin3 R451C knockin.

Specific structures, like the hippocampus, have long been reported as a region of interest in autism [Aylward et al., 1999]. In this study, we found a 12% decrease in the overall size of the hippocampus. This difference was consistent with the overall difference in volume, since there was no relative volume difference between groups. While this may indicate that the hippocampal difference is related to the total brain volume change, there are reported differences in these NL3 KI mice and the NL3 KO with hippocampal learning tasks [Radyushkin et al., 2009; Tabuchi et al., 2007]. Furthermore, one of the hallmark behaviors in autism is the repetitive restrictive behaviors, and these behaviors have often been thought to be associated with the striatum [Sears et al., 1999], which was determined to be 12% smaller in the NL3 KI mouse. In human autism, the striatum has been reported to be larger by some groups [Hollander et al., 2005; Rojas et al., 2006] but there was some concern over whether medication was a factor in the enlargement [Chakos et al., 1994]. Regardless, the smaller striatal volume in the NL3 KI is quite striking and is clearly affected by the genetic differences in the NL3 KI mouse.

As mentioned above, the NL3 KI mouse also had 10% less (FDR = 0.06) white matter than the wild type. The corpus callosum changes are intriguing as there is a history of corpus callosum changes in autism. Recent review articles and meta-analyses have pointed out a reduction in corpus callosum size in autism in humans [Cody, Pelphrey, & Piven, 2002; Stanfield et al., 2008; Verhoeven, De Cock, Lagae, & Sunaert, 2010]. This seems to be consistent with our findings of a −14% absolute volume difference (FDR = 0.03) in corpus callosum (as well as a −7% relative volume difference, FDR = 0.002). In the late 1990s, it was reported that the corpus callosum was reduced in size, particularly in the posterior regions [Egaas, Courchesne, & Saitoh, 1995; Piven, Bailey, Ranson, & Arndt, 1997]. Significantly smaller areas in the corpus callosum can be seen in Figure 3, which seem to be localized in the posterior in the NL3 KI along the midline, similar to previous findings in human autism [Egaas et al., 1995; Piven et al., 1997].

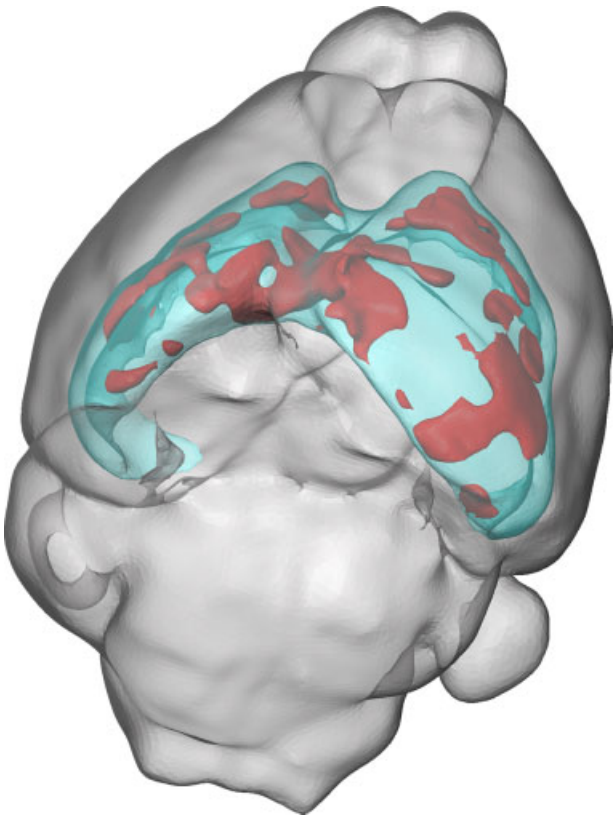

Figure 3. 3D representation of the mouse brain (in gray) showing a surface rendering of the corpus callosum (in blue). The areas where the volume of the NL3 KI mouse were smaller than the wild type (<10% false discovery rate) within the corpus callosum are highlighted in red. NL3 KI, neuroligin3 R451C knockin.

Using DTI, the underlying microstructure of the white matter can be examined. To reiterate, FA is a measure the amount of order in tissue. White matter structures have high FA values (i.e. preferred orientation, FA = 0.7–1.0), and gray matter structures or ventricles have low FA values (i.e. no preferred orientation, or spherically symmetric FA < 0.5). A smaller FA can be caused by a difference in the preferred orientation in the tissue, whereas in white matter this can be caused by less myelination, less axons (not as densely packed), or more random orientation of axons. Since no significant differences were found in the mean FA values in any of the white matter structures, but they still had significantly smaller volumes, it is reasonable to assume that the smaller volume in the NL3 KI is not due to a breakdown in the microstructure of the tissue and caused instead by a reduced number axons, or perhaps less oriented or less mature axons in the white matter regions with similar axonal density and microstructure. The corpus callosum in human autism has been reported as having a reduced FA value [Alexander, Lee, Lazar, Boudos et al., 2007b]; however, these authors also mention that the mechanism behind this change remains unclear. All the white matter changes found in the NL3 KI mouse seem to indicate that there is a reduced connectivity in the brain, which is consistent with what has been shown in human autism [Hughes, 2007].

Examining the FA differences on a voxel-by-voxel basis at an FDR threshold of 20% highlighted smaller FA values bilaterally in the globus pallidus of the NL3 KI mouse (Fig. 1B); moreover, there was a stronger change in FA in the right hemisphere (FDR < 0.10 at the peak). The fact that this difference was bilateral gave us more confidence in the FA difference in that region despite the 20% FDR, and allowed further investigation into the changes. While there was no absolute or relative volume change in the globus pallidus as a whole, the absolute volume of the right globus pallidus was found to be smaller in the NL3 KI (−10%, FDR = 0.09), which is consistent with the greater FA effect in that region, whereas there was no significant change in the left (FDR = 0.26). An FA change in the gray matter structure is a difficult interpretation. Since the globus pallidus is traversed by many myelinated axons with connections to putamen and the thalamus, it is reasonable to conclude that the smaller FA value in the NL3 KI compared and WT may indicate that there is a more coherent organization of those axons/connections in the globus pallidus in the WT mouse. A smaller bilateral FA in the globus pallidus has been found in a schizophrenic population, and the authors have a similar interpretation for the smaller FA. They suspected that there was damage to the myelinated nerve fibers traversing the globus pallidus [Hashimoto et al., 2009]. However, the FA changes found in the globus pallidus in this study were on the borderline of significance, and therefore, this finding needs to be replicated or investigated further.

In order to examine the microstructure of the tissue in more detail, the MD, AD, and RD were also assessed. Again, to reiterate, MD provides a measure of the diffusion of water averaged over all direction in the given space. AD and RD assess how the water molecules are traveling in relation to the underlying cellular environment, with AD measuring the principal direction of travel (i.e. parallel to the white matter tracts), and RD measuring the average diffusion orthogonal to the principal direction (i.e. perpendicular to the white matter tracts). No significant differences were found in the MD or AD in any of the 62 volumes or on a voxel-by-voxel basis, and despite the relative lack of FA, MD, and AD changes, significantly larger RD values were found (Fig. 2). A change in RD when there is no change in AD, should directly affect MD. However, in this study the changes in RD, although significant, are quite small. Given the variances in the MD and AD measures, the MD, while trending larger in a similar pattern as the RD (data not shown), did not reach significance in those same

areas. Interestingly, in the voxel-wise analysis there were strong changes in the RD of the corpus callosum, which may relate to the volume changes, since they were similarly located in the posterior of the corpus callosum (Fig. 2, right). Also, the larger RD in the cerebellum is intriguing, as there was no change in volume or FA in that area. A larger RD can be caused by a variety of reasons, some of which are: (1) myelin loss, (2) less aligned axons, and (3) a decrease in the axonal density; however, the differences in this study are subtle enough to not affect the FA or MD values, so therefore, whatever is driving the RD differences is quite subtle. In 1988, Courchesne et al. reported a hypoplasia of the vermian lobules in the cerebellum [Courchesne, Yeung-Courchesne, Press, Hesselink, & Jernigan, 1988], which has also been found in post mortem studies [Murakami, Courchesne, Press, Yeung-Courchesne, & Hesselink, 1989]. This reported hypoplasia of the cerebellum, could certainly be the cause of the differences in RD (i.e. immature myelination, or immature axons affecting density and size), and likewise may not affect the overall volume of the structure. Similar hypoplasia in the corpus callosum in human autism has also been found [Egaas et al., 1995].

It should be noted that imaging of fixed brain tissue has its pros and cons. For MR imaging, it allows one to get extremely detailed and high-resolution images, which is beneficial for both the volumetric and DTI measurements made in this study, whereas live imaging suffers from motion artifacts and short scanning sessions, which lead to poorer resolution. A typical live imaging session can only last a maximum of 3 hr, due to anesthesia constraints, whereas the scanning performed in this study requires 12–16 hr to complete. One of the concerns with fixed brain imaging is possible changes in the actual volume, due to the fixation process. However, the brains in this work are well hydrated and kept within the skull to eliminate any possible volume changes due to the fixation process. Benveniste and Blackband [2006] give a nice review of magnetic resonance microscopy in translational neuroscience. In that review, they highlight the benefits of measuring volume with fixed samples over in vivo. The main benefit discussed is that fixed brain imaging allows a more accurate delineation of the borders of the different structures due to the enhanced contrast (as MRI contrast agents are easily utilized for fixed brain imaging) and resolution compared to in vivo. In a DTI study, the diffusion characteristics of the brain are drastically altered in fixed brain tissue. The diffusion of water in the brain drops to 30–50% of its value in live animals [D'Arceuil & de Crespigny, 2007]. This does not allow accurate measurements of the diffusion coefficients in the brain. However, for the purposes of this work, in which we are focusing on the comparison between groups, the diffusion differences do not depend on the diffusion coefficients. Moreover, FA has been determined to be conserved in fixed brain tissue, providing that the tissue is fixed premortem or directly postmortem [D'Arceuil & de Crespigny, 2007].

Conclusions

This study reports a method for quantitative whole brain assessments of the volume and underlying tissue microstructure in a mouse model of autism. Consequently, marked volume differences in many different structures in the brain of the NL3 KI mouse model were found, a number of which are directly related to changes seen in human autism. The most intriguing finding in this study was that the large white matter volume differences were independent of a change in FA. This indicates that the volume differences found in the white matter regions are not due to a general breakdown in the microstructure of the tissue and seem to be caused by fewer or less mature axons. Further, the corpus callosum changes are particularly interesting as the thinning (or reduced volume) of the corpus callosum is a consistent finding across autism studies, which suggests that the NL3 KI model may be a useful model for examining white matter changes and the underconnectivity associated with autism.

Acknowledgments

This study was supported by the Canadian Institute for Health Research (Operating), and the Ontario Mental Health Foundation (Salary, J.E.).

References

Abrahams, B.S., & Geschwind, D.H. (2010a). Connecting genes to brain in the autism spectrum disorders. Archives of Neurology, 67, 395–399.

Abrahams, B.S., & Geschwind, D.H. (2010b). Genetics of autism. In: Speicher MR, Antonarakis SE, Motulsky AG, editors. Human genetics: problems and approaches, 4e. Heidelberg, Germany: Springer. p 699–714.

Alexander, A.L., Lee, J.E., Lazar, M., & Field, A.S. (2007). Diffusion tensor imaging of the brain. Neurotherapeutics, 4, 316–329.

Alexander, A.L., Lee, J.E., Lazar, M., Boudos, R., DuBray, M.B., et al. (2007). Diffusion tensor imaging of the corpus callosum in Autism. Neuroimage, 34, 61–73.

Aylward, E.H., Minshew, N.J., Goldstein, G., Honeycutt, N.A., Augustine, A.M., et al. (1999). MRI volumes of amygdala and hippocampus in non-mentally retarded autistic adolescents and adults. Neurology, 53, 2145–2150.

Bailey, A., Le Couteur, A., Gottesman, I., Bolton, P., Simonoff, E., et al. (1995). Autism as a strongly genetic disorder: Evidence from a British twin study. Psychological Medicine, 25, 63–77.

Baird, G., Simonoff, E., Pickles, A., Chandler, S., Loucas, T., et al. (2006). Prevalence of disorders of the autism spectrum in a

population cohort of children in South Thames: The Special Needs and Autism Project (SNAP). Lancet, 368, 210–215.
Benveniste, H., & Blackband, S.J. (2006). Translational neuroscience and magnetic-resonance microscopy. Lancet Neurology, 5, 536–544.
Bock, N.A., Nieman, B.J., Bishop, J.B., & Mark Henkelman, R. (2005). In vivo multiple-mouse MRI at 7 Tesla. Magnetic Resonance in Medicine, 54, 1311–1316.
Chadman, K.K., Gong, S., Scattoni, M.L., Boltuck, S.E., Gandhy, S.U., et al. (2008). Minimal aberrant behavioral phenotypes of neuroligin-3 R451C knockin mice. Autism Research, 1, 147–158.
Chakos, M.H., Lieberman, J.A., Bilder, R.M., Borenstein, M., Lerner, G., et al. (1994). Increase in caudate nuclei volumes of first-episode schizophrenic patients taking antipsychotic drugs. American Journal of Psychiatry, 151, 1430–1436.
Cody, H., Pelphrey, K., & Piven, J. (2002). Structural and functional magnetic resonance imaging of autism. International Journal of Developmental Neuroscience, 20, 421–438.
Collins, D.L., Neelin, P., Peters, T.M., & Evans, A.C. (1994). Automatic 3D intersubject registration of MR volumetric data in standardized Talairach space. Journal of Computer Assisted Tomography, 18, 192–205.
Courchesne, E., Yeung-Courchesne, R., Press, G.A., Hesselink, J.R., & Jernigan, T.L. (1988). Hypoplasia of cerebellar vermal lobules VI and VII in autism. New England Journal of Medicine, 318, 1349–1354.
D'Arceuil, H., & de Crespigny, A. (2007). The effects of brain tissue decomposition on diffusion tensor imaging and tractography. Neuroimage, 36, 64–68.
Dorr, A.E., Lerch, J.P., Spring, S., Kabani, N., & Henkelman, R.M. (2008). High resolution three-dimensional brain atlas using an average magnetic resonance image of 40 adult C57Bl/6J mice. Neuroimage, 42, 60–69.
Egaas, B., Courchesne, E., & Saitoh, O. (1995). Reduced size of corpus callosum in autism. Archives of Neurology, 52, 794–801.
Ellegood, J., Pacey, L.K., Hampson, D.R., Lerch, J.P., & Henkelman, R.M. (2010). Anatomical phenotyping in a mouse model of fragile X syndrome with magnetic resonance imaging. Neuroimage, 53, 1023–1029.
Fombonne, E. (2005). Epidemiology of autistic disorder and other pervasive developmental disorders. Journal of Clinical Psychiatry, 66, 3–8.
Genovese, C.R., Lazar, N.A., & Nichols, T. (2002). Thresholding of statistical maps in functional neuroimaging using the false discovery rate. Neuroimage, 15, 870–878.
Hashimoto, R., Mori, T., Nemoto, K., Moriguchi, Y., Noguchi, H., et al. (2009). Abnormal microstructures of the basal ganglia in schizophrenia revealed by diffusion tensor imaging. World Journal of Biological Psychiatry, 10, 65–69.
Henkelman, R.M., Baghdadi, L., & Sled, J.G. (2006). Presentation of 3D isotropic imaging data for optimal viewing. Magnetic Resonance in Medicine, 56, 1371–1374.
Hollander, E., Anagnostou, E., Chaplin, W., Esposito, K., Haznedar, M.M., et al. (2005). Striatal volume on magnetic resonance imaging and repetitive behaviors in autism. Biological Psychiatry, 58, 226–232.
Hughes, J.R. (2007). Autism: The first firm finding = underconnectivity? Epilepsy Behavior, 11, 20–24.
Jamain, S., Quach, H., Betancur, C., Rastam, M., Colineaux, C., et al. (2003). Mutations of the X-linked genes encoding neuroligins NLGN3 and NLGN4 are associated with autism. Nature Genetics, 34, 27–29.
Kirov, G., Gumus, D., Chen, W., Norton, N., Georgieva, L., et al. (2008). Comparative genome hybridization suggests a role for NRXN1 and APBA2 in schizophrenia. Human Molecular Genetics, 17, 458–465.
Lau, J.C., Lerch, J.P., Sled, J.G., Henkelman, R.M., Evans, A.C., & Bedell, B.J. (2008). Longitudinal neuroanatomical changes determined by deformation-based morphometry in a mouse model of Alzheimer's disease. Neuroimage, 42, 19–27.
Laumonnier, F., Bonnet-Brilhault, F., Gomot, M., Blanc, R., David, A., et al. (2004). X-linked mental retardation and autism are associated with a mutation in the NLGN4 gene, a member of the neuroligin family. American Journal of Human Genetics, 74, 552–557.
Lawson-Yuen, A., Saldivar, J.S., Sommer, S., & Picker, J. (2008). Familial deletion within NLGN4 associated with autism and Tourette syndrome. European Journal of Human Genetics, 16, 614–618.
Le Bihan, D., Mangin, J.F., Poupon, C., Clark, C.A., Pappata, S., et al. (2001). Diffusion tensor imaging: Concepts and applications. Journal of Magnetic Resonance Imaging, 13, 534–546.
Lerch, J.P., Carroll, J.B., Spring, S., Bertram, L.N., Schwab, C., et al. (2008). Automated deformation analysis in the YAC128 Huntington disease mouse model. Neuroimage, 39, 32–39.
Lerch, J.P., Yiu, A.P., Martinez-Canabal, A., Pekar, T., Bohbot, V.D., et al. (2011). Maze training in mice induces MRI-detectable brain shape changes specific to the type of learning. Neuroimage, 54, 2086–2095.
Murakami, J.W., Courchesne, E., Press, G.A., Yeung-Courchesne, R., & Hesselink, J.R. (1989). Reduced cerebellar hemisphere size and its relationship to vermal hypoplasia in autism. Archives of Neurology, 46, 689–694.
Nag, N., Moriuchi, J.M., Peitzman, C.G., Ward, B.C., Kolodny, N.H., & Berger-Sweeney, J.E. (2009). Environmental enrichment alters locomotor behaviour and ventricular volume in Mecp2 1lox mice. Behavioral Brain Research, 196, 44–48.
Nieman, B.J., Flenniken, A.M., Adamson, S.L., Henkelman, R.M., & Sled, J.G. (2006). Anatomical phenotyping in the brain and skull of a mutant mouse by magnetic resonance imaging and computed tomography. Physiological Genomics, 24, 154–162.
Piven, J., Bailey, J., Ranson, B.J., & Arndt, S. (1997). An MRI study of the corpus callosum in autism. American Journal of Psychiatry, 154, 1051–1056.
Radyushkin, K., Hammerschmidt, K., Boretius, S., Varoqueaux, F., El-Kordi, A., et al. (2009). Neuroligin-3-deficient mice: Model of a monogenic heritable form of autism with an olfactory deficit. Genes Brain and Behavior, 8, 416–425.
Reiss, A.L. (2009). Childhood developmental disorders: An academic and clinical convergence point for psychiatry, neurology, psychology and pediatrics. Journal of Child Psychology and Psychiatry, 50, 87–98.

Rojas, D.C., Peterson, E., Winterrowd, E., Reite, M.L., Rogers, S.J., & Tregellas, J.R. (2006). Regional gray matter volumetric changes in autism associated with social and repetitive behavior symptoms. BMC Psychiatry, 6, 56.

Sears, L.L., Vest, C., Mohamed, S., Bailey, J., Ranson, B.J., & Piven, J. (1999). An MRI study of the basal ganglia in autism. Progress in Neuro-psychopharmacol and Biological Psychiatry, 23, 613–624.

Spring, S., Lerch, J.P., & Henkelman, R.M. (2007). Sexual dimorphism revealed in the structure of the mouse brain using three-dimensional magnetic resonance imaging. Neuroimage, 35, 1424–1433.

Spring, S., Lerch, J.P., Wetzel, M.K., Evans, A.C., & Henkelman, R.M. (2010). Cerebral asymmetries in 12-week-old C57Bl/6J mice measured by magnetic resonance imaging. Neuroimage, 50, 409–415.

Stanfield, A.C., McIntosh, A.M., Spencer, M.D., Philip, R., Gaur, S., & Lawrie, S.M. (2008). Towards a neuroanatomy of autism: A systematic review and meta-analysis of structural magnetic resonance imaging studies. European Journal of Psychiatry, 23, 289–299.

Steffenburg, S., Gillberg, C., Hellgren, L., Andersson, L., Gillberg, I.C., et al. (1989). A twin study of autism in Denmark, Finland, Iceland, Norway and Sweden. Journal of Child Psychology and Psychiatry, 30, 405–416.

Tabuchi, K., Blundell, J., Etherton, M.R., Hammer, R.E., Liu, X., et al. (2007). A neuroligin-3 mutation implicated in autism increases inhibitory synaptic transmission in mice. Science, 318, 71–76.

Verhoeven, J.S., De Cock, P., Lagae, L., & Sunaert, S. (2010). Neuroimaging of autism. Neuroradiology, 52, 3–14.

Zahir, F.R., Baross, A., Delaney, A.D., Eydoux, P., Fernandes, N.D., et al. (2008). A patient with vertebral, cognitive and behavioural abnormalities and a de novo deletion of NRXN1alpha. Journal of Medical Genetics, 45, 239–243.